Amino Acids (2015) 47:937–948
DOI 10.1007/s00726-015-1923-3

ORIGINAL ARTICLE

Oligomeric state and structural stability of two hyperthermophilic β-glucosidases from *Thermotoga petrophila*

Francieli Colussi · Viviam M. da Silva · Ian Miller · Junio Cota · Leandro C. de Oliveira · Mário de Oliveira Neto · Fábio M. Squina · Wanius Garcia

Received: 25 June 2014 / Accepted: 15 January 2015 / Published online: 31 January 2015

Abstract The β-glucosidases are enzymes essential for several industrial applications, especially in the field of plant structural polysaccharides conversion into bioenergy and bioproducts. In a recent study, we have provided a biochemical characterization of two hyperthermostable β-glucosidases from *Thermotoga petrophila* belonging to the families GH1 (*Tp*BGL1) and GH3 (*Tp*BGL3). Here, as part of a continuing investigation, the oligomeric state, the net charge, and the structural stability, at acidic pH, of the *Tp*BGL1 and *Tp*BGL3 were characterized and compared. Enzymatic activity is directly related to the balance between protonation and conformational changes. Interestingly, our results indicated that there were no significant changes in the secondary, tertiary and quaternary structures of the β-glucosidases at temperatures below 80 °C. Furthermore, the results indicated that both the enzymes are stable homodimers in solution. Therefore, the observed changes in the enzymatic activities are due to variations in pH that modify protonation of the enzymes residues and the net charge, directly affecting the interactions with ligands. Finally, the results showed that the two β-glucosidases displayed different pH dependence of thermostability at temperatures above 80 °C. *Tp*BGL1 showed higher stability at pH 6 than at pH 4, while *Tp*BGL3 showed similar stability at both pH values. This study provides a useful comparison of the structural stability, at acidic pH, of two different hyperthermostable β-glucosidases and how it correlates with the activity of the enzymes. The information described here can be useful for biotechnological applications in the biofuel and food industries.

Keywords β-Glucosidase · Cellulose · Biomass · *T. petrophila* · Hyperthermostable · Biofuels

Handling Editor: C. Schiene-Fischer.

F. Colussi and V. M. da Silva have contributed equally to this work.

Electronic supplementary material The online version of this article (doi:10.1007/s00726-015-1923-3) contains supplementary material, which is available to authorized users.

F. Colussi · V. M. da Silva · I. Miller · W. Garcia (✉)
Centro de Ciências Naturais e Humanas (CCNH), Universidade Federal do ABC (UFABC), Santo André, SP, Brazil
e-mail: wanius.garcia@ufabc.edu.br

J. Cota · F. M. Squina
Laboratório Nacional de Ciência e Tecnologia do Bioetanol, Centro Nacional de Pesquisa em Energia e Materiais, Campinas, SP, Brazil

L. C. de Oliveira
Departamento de Física, Instituto de Biociências, Letras e Ciências Exatas, UNESP Univ Estadual Paulista, São José do Rio Preto, SP, Brazil

M. de Oliveira Neto
Departamento de Física e Biofísica, Instituto de Biociências, UNESP Univ Estadual Paulista, Botucatu, SP, Brazil

Introduction

The most promising conversion technology for lignocellulosic biomass is based on the enzymatic hydrolysis of its cellulose fraction to glucose, followed by microbial fermentation of the glucose to ethanol (Kumar et al. 2008; Rezende et al. 2011). The enzymatic hydrolysis of cellulose to glucose requires at least three kinds of cellulases working synergistically: endoglucanases (EC 3.2.1.4), cellobiohydrolases (EC 3.2.1.91) and β-glucosidases (EC 3.2.1.21) (Lynd et al. 2002; Colussi et al. 2012). The endoglucanases

randomly cut cellulose chains in amorphous regions, where they are easily accessible, into shorter fragments of several lengths. The cellobiohydrolases cleave off cellobiose units from the reducing or nonreducing end of cellulose chains in the less-accessible crystalline regions. Lastly, the β-glucosidases hydrolyze the released cellodextrin and cellobiose to glucose (Lynd et al. 2002; Sørensen et al. 2013). The endoglucanases and cellobiohydrolases are often inhibited by cellobiose, making β-glucosidases important in terms of avoiding decreased hydrolysis rates of cellulose over time due to cellobiose accumulation (Shewale 1982; Xiao et al. 2004; Sørensen et al. 2013). Thus, the study of β-glucosidases has been strongly stimulated, especially in the field of plant structural polysaccharides conversion into bioenergy and bioproducts (Lynd et al. 2008).

The β-glucosidases have been classified into glycoside hydrolase (GH) families GH1, GH3, GH5, GH9, GH30 and GH116, based on their amino acid sequences and three-dimensional structures (Lombard et al. 2013; Cairns and Esen 2010; Sørensen et al. 2013). The families GH1, GH5, and GH30 belong to the Clan GH-A, and they all have similar $(\beta/\alpha)_8$-barrel domains that contain their active site, while GH9 enzymes have $(\alpha/\alpha)_6$-barrel structures (Cairns and Esen 2010). The GH1 have a $(\beta/\alpha)_8$-barrel structure and its active site contain two conserved carboxylic acid residues on β-strands four and seven, serving as the catalytic acid/base and nucleophile, respectively (Cairns and Esen 2010). The GH3 β-glucosidases have a two-domain structure, a $(\beta/\alpha)_8$-barrel followed by an α/β sandwich comprising a 6-stranded β-sheet sandwiched between three α-helices on either side. The active site of GH3 enzymes is situated between the $(\beta/\alpha)_8$ and $(\alpha/\beta)_6$ sandwich domains, each of which contributes one catalytic carboxylate residue.

Thermotoga petrophila strain RKU-1 (T) is a hyperthermophilic bacterium isolated from the Kubiki oil reservoir in Niigata (Japan) that grows optimally at 80 °C (Takahata et al. 2001). Some hyperthermostable enzymes produced by this microorganism have demonstrated great potential for industrial applications and served as models to investigate structure–function–stability relationships in glycosyl hydrolases (Santos et al. 2011; Cota et al. 2011; Santos et al. 2012; Silva et al. 2014). For industrial purposes, an enzyme of thermophilic origin can be considered favorable, since elevated temperatures can yield higher substrate solubility, lower viscosity, and thereby lower pumping costs, and limited risks of bacterial contamination (Lundemo et al. 2013).

In a recent study, we have provided a biochemical characterization of two hyperthermostable β-glucosidases from *T. petrophila* belonging to the families GH1 (*Tp*BGL1) and GH3 (*Tp*BGL3) (Cota et al. 2015). Here, as part of a continuing investigation, the oligomeric state, the net charge, and the structural stability, at acidic pH, of the *Tp*BGL1 and *Tp*BGL3 were characterized and compared. The study described here provides a useful comparison of the structural stability, at acidic pH, of two different hyperthermostable β-glucosidases and how it correlates with the activity of the enzymes. Also, the information described in this study can be useful for biotechnological applications.

Materials and methods

Materials

Imidazole, kanamycin, LB medium, isopropyl-β-D-thiogalactopyranoside (IPTG) and nickel–nitrilotriacetic acid resin (Ni–NTA) were purchased from Sigma-Aldrich. Protein standards used as sodium dodecyl sulfate-polyacrylamide gel electrophoresis (SDS-PAGE) markers were from Sigma. All chemicals and reagents used in this study were of the highest purity analytical grade.

Cloning, expression and purification of recombinant *Tp*BGL1 and *Tp*BGL3

Cloning, expression and purification of the *Tp*BGL1 (GenBank: ABQ46970.1) and *Tp*BGL3 (GenBank: ABQ46916.1) were carried out as described previously (Cota et al. 2015; Squina et al. 2009). The purity of the final products, *Tp*BGL1 and *Tp*BGL3, were checked by Coomassie-stained 15 % SDS-PAGE. *Tp*BGL1 and *Tp*BGL3 concentrations were determined by UV absorbance at 280 nm using a theoretical extinction coefficient based on the amino acid composition. The extinction coefficients were calculated for the monomers using the ProtParam tool (http://web.expasy.org/protparam). The theoretical coefficients employed were $\varepsilon_{280nm} = 121{,}240\ M^{-1}cm^{-1}$ for *Tp*BGL1 and $\varepsilon_{280nm} = 102{,}930\ M^{-1}cm^{-1}$ for *Tp*BGL3. The final purified products were then frozen and stored at −80 °C and were melted on ice before use.

Enzymatic activity measurements

The standard enzymatic assay for β-glucosidase activities was performed according to previously described method (Cota et al. 2015). 100 ng of enzyme, 40 µL of buffer solution adjusted at different pH values (pH range between 2 and 10) were used and 50 µL of 1 mM 4-nitrophenyl-β-D-glucopyranoside (*p*NPG) was used as substrate. Following incubation at 70 °C during 4 min, the reaction was stopped by addition of 100 µL of 1 M Na_2CO_3 and the releasing of *p*-nitrophenol was monitored colorimetrically at 405 nm using an Infinite 200 PRO microplate reader 20 (TECAN). All the enzyme assays were carried out employing the automated pipetting system epMotion 5075 (Eppendorf). One

unit of β-glucosidase activity was defined as the amount of enzyme that released *p*-nitrophenol at rate of 1 μmol min^{-1} under standard conditions. All experiments were done in triplicate, and average values are reported.

Far-UV circular dichroism (CD) spectroscopy

Far-UV CD spectra were collected using a Jasco J-815 spectropolarimeter equipped with a temperature control device. *Tp*BGL1 and *Tp*BGL3 concentrations were 0.25 mg mL^{-1} in 20 mM acetate–borate–phosphate buffer adjusted to the different pH values (pH 6 and 4). All data were collected at 20 °C using 0.1 cm quartz cuvette and the spectra were recorded over the wavelength range from 195 to 260 nm. Eight accumulations were averaged to form the CD spectra, using a scanning speed of 100 nm min^{-1}, a spectral bandwidth of 1 nm, and a response time of 0.5 s, and obtained on degree scale. The buffer contribution was subtracted in each of the experiments. Spectra were transformed to molar ellipticity (θ) using the mean weight residue and concentration prior to the secondary-structure analysis. Thermal unfolding of *Tp*BGL1 and *Tp*BGL3 (0.25 mg mL^{-1}) were characterized by measuring the ellipticity changes at 222 nm at different pH values (pH 6 and 4) induced by a temperature increase from 50 to 100 °C at a heating rate of 10 °C h^{-1}. Specifically, the temperature of the samples were increased by 5 °C over a period of 5 min followed by a rest period of a further 5 min, leading to a total of 10 min per data point. The ellipticity data obtained from the studies of thermal denaturation were analyzed assuming an irreversible transition process.

Dynamic light scattering (DLS)

The size characteristics of the purified *Tp*BGL1 and *Tp*BGL3 samples were examined by means of the Nano-ZS dynamic light scattering system (Malvern Instruments Ltd, Malvern, UK) (Hall et al. 2011). This system employs a 633 nm laser and a fixed scattering angle (173°). Protein solutions (1 mg mL^{-1}), in 20 mM acetate–borate–phosphate buffer adjusted at pH 6 or 4, were first passed through a 0.22 μm filter (Millipore, USA), centrifuged at 16,000×*g* for 10 min at room temperature, and subsequently loaded into a quartz cuvette prior to measurement. The temperature was raised from 20 to 90 °C and the samples were allowed to equilibrate for 5 min in each temperature prior to DLS measurements, after which multiple records of the DLS profile were collected. In a second experiment which included temperatures above 90 °C, the samples were incubated for 5 min at 100 °C and subsequently cooled to 20 °C, and then the samples were measured as described above. In each case the hydrodynamic radius (R_s) was obtained from a second-order cumulant fit to the intensity auto-correlation function (size distribution by volume). The marked point where both the size and the intensity start to increase significantly is called the melting point. In each case, the determined R_s was converted to molecular mass (kilo-Daltons) on the basis of the assumption of a spherical particle and using the Zetasizer software.

Electrophoretic light scattering (ELS)

Electrophoretic light scattering (ELS) measurements were used to determine the average zeta potential (ζ) of the enzymes, which were collected using a Zetasiser Nano-ZS at 20 °C (Jachimska et al. 2008; Santiago et al. 2010). In this study, the zeta potential was measured for a fixed protein concentration (*Tp*BGL1 and *Tp*BGL3) of 1 mg mL^{-1} (at 20 °C) in 20 mM acetate–borate–phosphate buffer adjusted to the different pH values. This instrument measures the electrophoretic mobility (μ_e) and converts the value to a ζ potential (mV) through Henry's equation: $\mu_e = [2\varepsilon\zeta F(\kappa a)]/3\eta$, where ε is the dielectric constant of water and η is the viscosity. Furthermore, $F(\kappa a)$ is the Henry's function, which was calculated through the Smoluchowski approximation $F(\kappa a) = 1.5$. The isoelectric point is given by the pH value at which the zeta potential is approximately zero. Knowledge of the electrophoretic mobility enables one to calculate the average number of charges per molecule (N_c) from the Lorenz–Stokes relationship $N_c = \frac{6\pi\eta}{e} R_s \mu_e$, where μ_e is expressed in μm cm s^{-1} V^{-1} and the value in the denominator corresponds to the elementary charge ($e = 1.602 \times 10^{-19}$ C) (Jachimska et al. 2008; Santiago et al. 2010).

Small-angle X-ray scattering (SAXS) data collection

The SAXS measurements were performed at the SAXS-2 beamline of LNLS (National Synchrotron Light Laboratory, Campinas, Brazil). For SAXS measurements, *Tp*BGL1 and *Tp*BGL3 were measured at different protein concentrations (1 and 5 mg mL^{-1} in 20 mM acetate–borate–phosphate buffer adjusted at pH 6 and 4). The samples were passed through a 0.22-μm filter (Millipore, USA) and centrifuged at 16,000x*g* for 10 min at room temperature prior to measurement. The samples were then loaded into a 1 mm path length cell made of two thin parallel mica windows. The sample temperature (at 20 °C) was controlled during the measurements. The wavelength of the incoming monochromatic X-ray beam was $\lambda = 1.55$ Å and the sample-to-detector distance was set at 0.95 m, providing a q (scattering vector) interval from 0.015 to 0.35 $Å^{-1}$, where $q = 4\ \pi\sin(\theta)/\lambda$ and θ is half the scattering angle. Two successive frames of 300 s were recorded for each sample to monitor radiation damage and beam stability. Buffer scattering was recorded before each sample

scattering. The X-ray patterns were recorded using a two-dimensional CCD detector (MarResearch, USA). The parasitic scattering from air and beam-line windows was subtracted from the total measured intensities. The integration of SAXS patterns were performed with the FIT2D software (www.esrf.eu/computing/scientific/FIT2D) and the curves were scaled by protein concentration. The scattering of water measured on the same sample cell was used to normalize the data to absolute scale. No concentration effects were detected for the samples.

SAXS data analysis, chemical analysis of interfaces and homology models

The radii of gyration (R_g) were determined by two independent procedures: (1) by the Guinier equation $I(q) = I(0)\exp[(-q^2.\ R_g^2)/3]$, $q < 1.3/R_g$, and (2) by the indirect Fourier transform method using the GNOM package (Svergun 1992). The distance distribution function $P(r)$ was also evaluated with GNOM software and the maximum diameter (D_{max}) was obtained. The CRYSOL package was used to generate theoretical scattering curves from tridimensional crystallographic structures (Svergun et al. 1995, Dias et al. 2013). The R_g and D_{max} of the tridimensional crystallographic structures were determined with the same package. We used the PISA server from the European Bioinformatics Institute (Krissinel and Henrick 2007) to calculate interface areas, free energy barrier of assembly dissociation (ΔG^{diss}) and the solvation free energy gain upon formation of the assembly (ΔG^{int}). The PISA server was employed to search for biological assemblies in the crystal structures [PDB 1OIN (Zechel et al. 2003) and PDB 2X41 (Pozzo et al. 2010)]. Figures were generated by the PyMol program (www.pymol.org). The three-dimensional models of the *Tp*BGL1 and *Tp*BGL3 were built by SWISS Model Server (Arnold et al. 2006) using as template the available structures of the β-glucosidases from *Thermotoga maritima* (*Tm*BGL1, PDB 1OIN) and *Thermotoga neapolitana* (*Tn*BGL3, PDB 2X41), respectively. The quality of the models was estimated using the index global model quality estimation (GMQE). The resulting GMQE index is expressed as a number between zero and one. Higher numbers indicate higher reliability.

Results and discussion

Expression, purification and enzymatic activity of the recombinant β-glucosidases

After successful expression in *E. coli*, the greater part of the recombinant enzymes, *Tp*BGL1 or *Tp*BGL3, were found

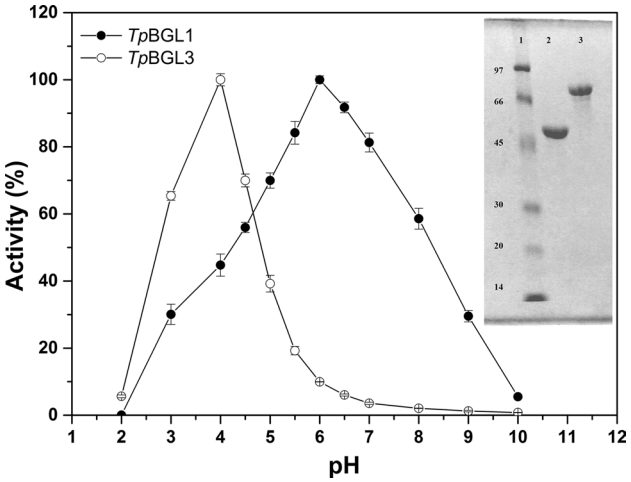

Fig. 1 Effect of pH on the enzymatic activity of *Tp*BGL1 (*filled circle*) and *Tp*BGL3 (*open circle*) at 70 °C. *Inset* Gel electrophoresis under denaturing conditions (15 % SDS-PAGE). Coomassie stained showing *Tp*BGL1 and *Tp*BGL3 enzymes after purification. Lane 1, molecular mass standards. Lane 2, *Tp*BGL1 (54 kDa). Lane 3, *Tp*BGL3 (84 kDa)

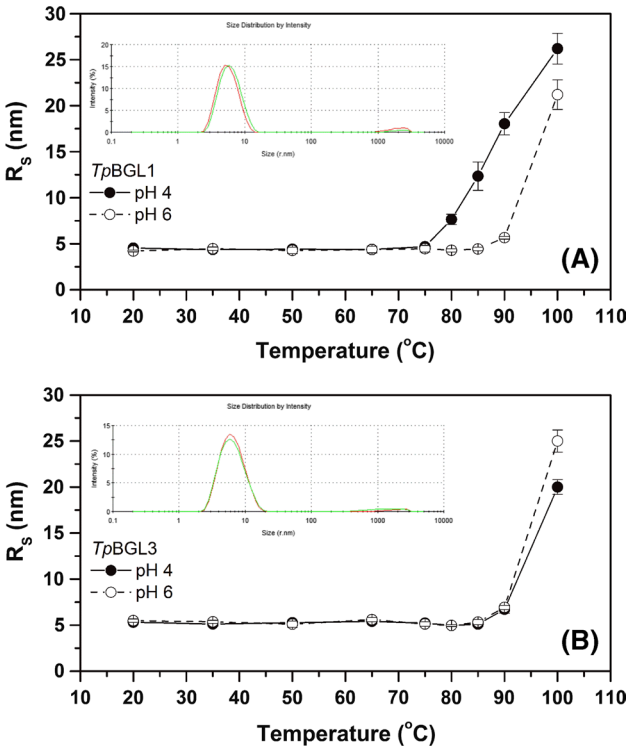

Fig. 2 Characterization of *Tp*BGL1 and *Tp*BGL3 by DLS. **a** R_S of *Tp*BGL1 as a function of temperature at pH 4 and 6. *Inset* the size distribution by intensity for purified *Tp*BGL1 (1 mg mL^{-1}) where DLS runs were conducted at pH 6 (*green line*) and 4 (*red line*). **b** R_S of *Tp*BGL3 as a function of temperature at pH 4 and 6. *Inset* the size distribution by intensity for purified *Tp*BGL3 (1 mg/mL) where DLS runs were conducted at pH 6 (*green line*) and 4 (*red line*). The *lines* are just a guide for the eye (color figure online)

in the supernatant after lysis. The recombinant enzymes were purified to apparent homogeneity by a two-step protocol using both affinity and size-exclusion chromatographies (Cota et al. 2015). Upon 15 % SDS-PAGE under reducing conditions the purified enzymes migrated as large homogenous bands, consistent with the expected molecular mass for *Tp*BGL1 (54 kDa) and *Tp*BGL3 (84 kDa) monomers (inset of Fig. 1). The final yields for the two purified enzymes per liter of culture medium were typically 20 and 15 mg for *Tp*BGL1 and *Tp*BGL3, respectively.

The β-glucosidase activity of *Tp*BGL1 and *Tp*BGL3 were studied as a function of pH (at 70 °C) using *p*NPG as substrate (Fig. 1). Our results showed that, under the conditions of our study, the activity of *Tp*BGL1 increases as pH increases within the pH 2–6 and then decreases within the pH 6–10. The enzyme *Tp*BGL1 reached its optimum activity around pH 6, while at pH 2 and 10 the remaining activities were virtually absent. In the case of *Tp*BGL3, the activity increases as pH increases within the pH range of 2-4 and then decreases within the pH 4–10 (Fig. 1). The enzyme *Tp*BGL3 reached its optimum activity around pH 4, while at pH 2 and pH values above 7 the remaining activities were virtually zero.

Recombinant β-glucosidases from *T. petrophila* are stable homodimers in solution

To obtain information about the tertiary structure of β-glucosidases, we submitted the enzymes to DLS analysis. When *Tp*BGL1 and *Tp*BGL3 were analyzed by DLS in solution at pH 6 and 4, the observed profiles were characteristic of monodisperse solutions (inset of Fig. 2). The values of R_s determined for *Tp*BGL1 at pH 4 and 6 were 4.5 ± 0.3 and 4.3 ± 0.3 nm, respectively (Fig. 2a). These values, corresponding to an estimated molecular mass (MM) of 113 and 102 kDa, are most consistent with a homodimer for *Tp*BGL1 in solution, whose expected MM is 108 kDa (the theoretical MM of a monomer is 54 kDa). For *Tp*BGL3, the values of R_S determined at pH 4 and 6 were 5.3 ± 0.2 and 5.5 ± 0.3 nm, respectively (Fig. 2b). These values, corresponding to an estimated MM of 167 and 182 kDa, are also most consistent with a homodimer for *Tp*BGL3 in solution, whose expected MM is 168 kDa (the theoretical MM of a monomer is 84 kDa).

To prove the conclusions suggested by the DLS results, we performed additional studies employing SAXS at the two pH values. The SAXS intensity profiles for *Tp*BGL1 measured at pH 6 and 4 (5 mg mL^{-1}) and the associated Guinier fits are shown in Fig. 3. The scattering data collected under the two solution conditions have a similar overall character, indicating that the gross features of the structures are similar. The Guinier plots are linear, suggesting that the molecules are free of significant intermolecule

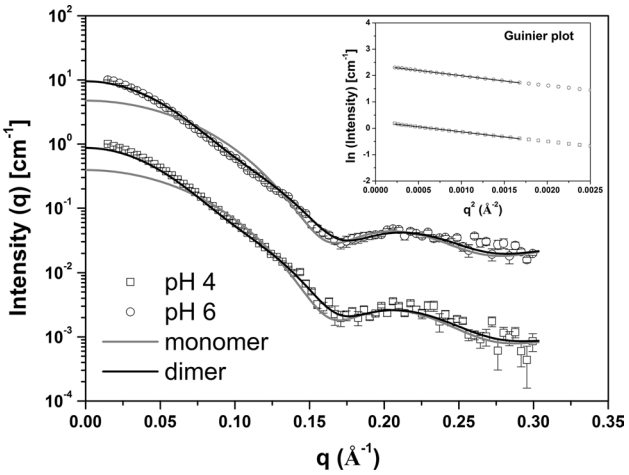

Fig. 3 SAXS data collected at 20 °C for *Tp*BGL1 at pH 6 and 4. Experimental SAXS *curves* of the *Tp*BGL1 at pH 6 (*circles* with *error bars*) and 4 (*squares* with *errors bars*) superimposed on the computed scattering *curve* based on the high-resolution homodimer (*black solid lines*) and high-resolution monomer (*gray solid lines*). The experimental *curves* have been offset for clarity. *Inset* Guinier plots (ln *I* vs. q^2) for *Tp*BGL1 at pH 6 (*circles*) and 4 (*squares*). The *curves* have been offset for clarity

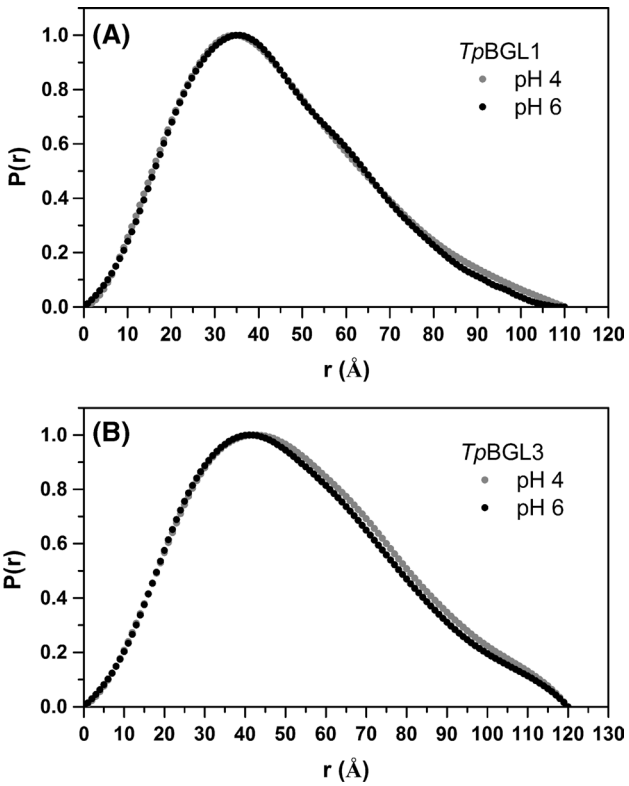

Fig. 4 Experimental distance distribution functions at 20 °C. **a** Experimental *P*(r) of *Tp*BGL1 at pH 6 (*black circles*) and 4 (*gray circles*). **b** Experimental *P*(r) of *Tp*BGL3 at pH 6 (*black circles*) and 4 (*gray circles*). The *curves* have been scaled to a maximum height of 1.0 for ready comparison

interference and aggregation. The radii of gyration (R_g) calculated with Guinier approximation at pH 6 and 4 were 33.92 ± 0.31 Å and 34.60 ± 0.25 Å, respectively. The R_g values determined at 1 and 5 mg mL^{-1} are similar (Table S1), which indicates that R_g is independent of protein concentrations used in these experiments. The distance distribution functions, $P(r)$, evaluated by the indirect Fourier transform with GNOM package (Svergun 1992) are shown in Fig. 4. The profiles have very similar shapes and trail off to a D_{max} of 110 ± 5 Å.

Oligomeric structures appear to be a common characteristic of GH1 family β-glucosidases (Aguilar et al. 1997; Chi et al. 1999; Zechel et al. 2003; Cairns and Esen 2010; Kado et al. 2011). Considering GH1 β-glucosidases from hyperthermophilic bacteria with structures determined experimentally, *Tp*BGL1 showed high sequential identity only when compared with GH1 β-glucosidase from *Thermotoga maritima* (*Tm*BGL1, 99 %) (Zechel et al. 2003). However, *Tp*BGL1 showed low sequential identity when compared with GH1 β-glucosidase from *Sulfolobus solfataricus* (*Ss*BGL1, 31 %) (Aguilar et al. 1997), *Thermosphaera aggregans* (*Ta*BGL1, 31 %) (Chi et al. 1999), and *Pyrococcus furiosus* (*Pf*BGL1, 26 %) (Kado et al. 2011). *Tm*BGL1 forms homodimers (Zechel et al. 2003), while *Ss*BGL1, *Ta*BGL1 and *Pf*BGL1 form homotetramers (Aguilar et al. 1997; Chi et al. 1999; Kado et al. 2011). The three-dimensional model of the *Tp*BGL1 built by SWISS Model Server (Arnold et al. 2006) using as template the structure of the *Tm*BGL1 (PDB 1OIN) (Zechel et al. 2003) showed excellent reliability (GMQE = 1, Fig. S1). In addition, we performed a search for biological assemblies in the crystal structure of *Tm*BGL1 (PDB 1OIN) using the PISA server (Krissinel and Henrick 2007). Only one stable homodimeric biological assembly was detected (Fig. 5a). The buried solvent-accessible surface (BSAS) of the homodimer interface was 1135 $Å^2$, and containing nine hydrogen bonds. The chemical stability of complex was analyzed by calculating the free energy barrier of assembly dissociation (ΔG^{diss}) and the solvation free energy gain upon formation of the assembly (ΔG^{int}) also using PISA server. The values determined were $\Delta G^{diss} = 3.0$ kJ mol^{-1} and $\Delta G^{int} = -5.4$ kJ mol^{-1}. The positive value obtained for ΔG^{diss} indicates that the homodimer is thermodynamically stable, and that an external driving force is required to dissociate the assembly (Tomovic and Oakeley 2008).

The Fig. 3 shows the experimental SAXS curves for *Tp*BGL1 measured at the two pH values superimposed on the computed scattering curve based on the homodimeric high-resolution structure detected by the PISA server (black solid lines). The theoretical scattering curve calculated from the homodimeric structure (Fig. 5a) gives a good fit to the scattering data at pH 6 ($\chi = 2.5$) and 4 ($\chi = 4.1$). However, the scattering curves calculated from the monomeric structure (Fig. 3, gray solid lines) gives a worse fit to the scattering data at pH 6 ($\chi = 7.8$) and 4 ($\chi = 9.0$). Therefore, it is clear that the SAXS data for *Tp*BGL1 at pH 6 and 4 are consistent with homodimeric molecules in solution. The homodimeric high-resolution structure shows a particle with a D_{max} of 105.8 Å and $R_g = 31.22$ Å (Fig. 5a). These values are in a good agreement with results obtained by SAXS analysis (Table S2). Furthermore, the SaxsmoW web tool (Fischer et al. 2010) was used to calculate the MM of *Tp*BGL1 and the values determined at pH 6 and 4 were 98.80 and 94.80 kDa, respectively. These results are also broadly consistent with a homodimer.

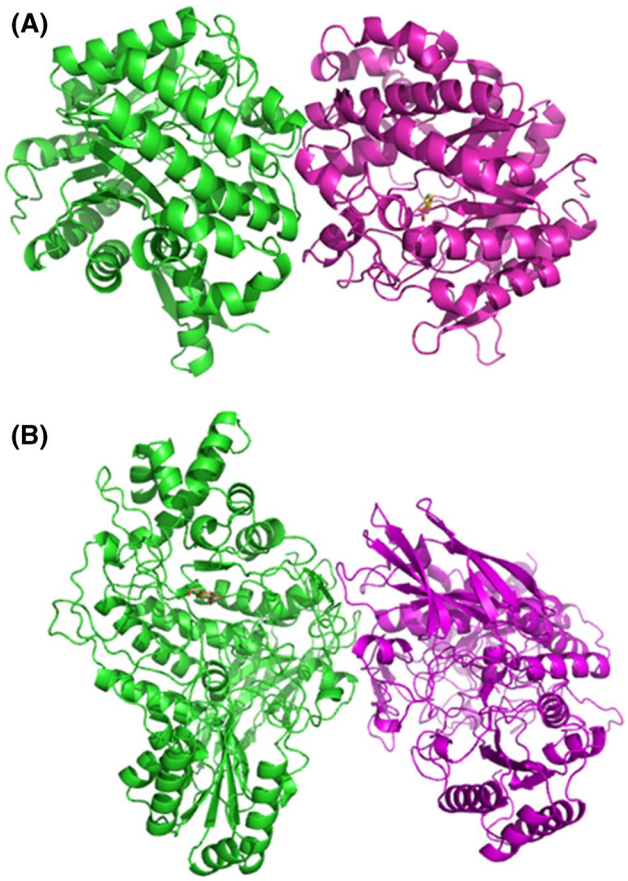

Fig. 5 High-resolution structures of the β-glucosidases. **a** *Tm*BGL1 high-resolution homodimer detected by the PISA server using the PDB 1OIN. **b** *Tn*BGL3 high-resolution homodimer detected by the PISA server using the PDB 2X41

In a previous study, we have demonstrated that at pH 6 and 99 °C *Tp*BGL1 presented a half-life at last ten times lower than that observed for *Pf*BGL1 (Cota et al. 2015). This difference in thermostability probably is due to the oligomerization state. Our SAXS results showed that *Pf*BGL1 forms a homotetramer in solution at pH 6 (Fig. S2), confirming previously published results (Kado et al. 2011). Thus, the chemical stability of the homotetramer (PDB

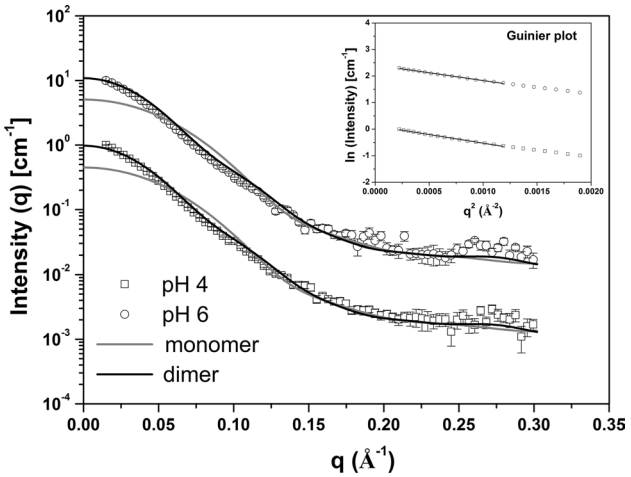

Fig. 6 SAXS data collected at 20 °C for *Tp*BGL3 at pH 6 and 4. Experimental SAXS *curves* of the *Tp*BGL3 at pH 6 (*circles* with *error bars*) and 4 (*squares* with *errors bars*) superimposed on the computed scattering *curve* based on the high-resolution homodimer (*black solid lines*) and high-resolution monomer (*gray solid lines*). The experimental *curves* have been offset for clarity. *Inset* Guinier plots (ln *I* vs. q^2) for *Tp*BGL3 at pH 6 (*circles*) and 4 (*squares*). The *curves* have been offset for clarity

3APG) (Kado et al. 2011) was analyzed by the employed PISA server (Krissinel and Henrick 2007). The BSAS determined was 4274 Å^2, containing 38 hydrogen bonds and 13 salt bridges. The values determined for ΔG^{diss} and ΔG^{int} were 7.3 and −35.4 kJ mol^{-1}, respectively. The values obtained for the BSAS and ΔG^{diss} are higher for the homotetramer than for the homodimer, indicating that *pf*BGL1 homotetramer is more thermodynamically stable than *Tp*BGL1 homodimer.

The X-ray scattering curves obtained for *Tp*BGL3 at pH 6 and 4 (5 mg mL^{-1}) and the associated Guinier fits are shown in Fig. 6. Again, the scattering data have a similar overall character, indicating that the gross features of the structures are similar. The Guinier plot of the data exhibited a linear behavior indicating excellent monodispersivity. The R_g values determined with Guinier approximation at pH 6 and 4 were 41.85 ± 0.66 and 40.38 ± 0.49 Å, respectively. The R_g values determined at 1 and 5 mg mL^{-1} are similar (Table S1), which indicates that R_g is independent of protein concentrations used in these experiments. The *P*(r) profiles evaluated with GNOM package (Svergun 1992), shown in Fig. 4b, have very similar shapes and trail off to a D_{max} of 120 ± 5 Å.

Crystal structures of GH3 family β-glucosidases have been reported for six enzymes: β-glucosidase from *Aspergillus aculeatus* (Suzuki et al. 2013), JMB19063 from switchgrass soil metagenome (McAndrew et al. 2013), exo-1,3/1,4-β-glucanase from *Pseudoalteromonas* sp. BB1 (Nakatani et al. 2012), β-glucosidase 3B from *Thermotoga neapolitana* (Pozzo et al. 2010), β-glucosidase from yeast *Kluyveromyces marxianus* (Yoshida et al. 2010) and β-D-glucan glucohydrolase ExoI from barley *Hordeum vulgare* (Varghese et al. 1999). Among these six β-glucosidases, GH3 β-glucosidase from *Thermotoga neapolitana* (*Tn*BGL3) (Pozzo et al. 2010) and JMB19063 from switchgrass soil metagenome (McAndrew et al. 2013) are most similar to *Tp*BGL3. *Tp*BGL3 showed 88 and 30 % amino acid sequence identity when compared with *Tn*BGL3 and JMB19063, respectively. Similar to *Tn*BGL3 and JMB19063, *Tp*BGL3 is a case of β-glucosidase arranged in three distinct domains. The N-terminal domain is an $(\alpha/\beta)_8$ triose phosphate isomerase (TIM) barrel, followed by a five-stranded α/β sandwich domain. The C-terminal domain has a fibronectin type III fold and is of unknown function, although it may be involved in the anchoring of the enzyme on large polymeric substrates and in thermostability (Pozzo et al. 2010). The three-dimensional model of the *Tp*BGL3 built by SWISS Model Server (Arnold et al. 2006) using as template the structure of the *Tn*BGL3 (PDB 2X41) (Pozzo et al. 2010) showed excellent reliability (GMQE = 0.96, Fig. S1). In the structure of *Tn*BGL3, only the first two domains have a direct role in the architecture of the active site and the oligomeric state is unknown (Pozzo et al. 2010). However, in the structure of JMB19063, the C-terminal domain from the opposing monomer composes a portion of the enzyme active site, and the dimerization is absolutely required for catalytic activity (McAndrew et al. 2013).

The PISA server was employed to search for biological assemblies in the crystal structure of *Tn*BGL3 (PDB 2X41). Again, only one stable homodimeric biological assembly was detected (Fig. 5b). The BSAS of the homodimer interface was 1260 Å^2, and containing 21 hydrogen bonds and 16 salt bridges. The values determined for ΔG^{diss} and ΔG^{int} were 3.6 and −93.6 kJ mol^{-1}, respectively. The positive value obtained for ΔG^{diss} indicates that the homodimer is thermodynamically stable. In the structure of JMB19063 (PDB 3U48), the BSAS of the homodimer interface was 3322 Å^2, containing 67 hydrogen bonds and 19 salt bridges (McAndrew et al. 2013). In addition, the values determined for ΔG^{diss} and ΔG^{int} were 33.5 and −34.2 kJ mol^{-1}, respectively. The values obtained for the BSAS and ΔG^{diss} are higher for JMB19063 than for *Tn*BGL3. Therefore, the results indicate that JMB19063 forms homodimers (Fig. S3) more thermodynamically stable than *Tn*BGL3, probably due to the dimerization to be absolutely required for catalytic activity.

The Fig. 6a shows the experimental SAXS curves for *Tp*BGL3 measured at the two pH values superimposed on the computed scattering curve based on the homodimeric structure detected by the PISA server (black solid lines). The theoretical scattering curves calculated from

the homodimeric structure (Fig. 5b) gives a good fit to the scattering data at pH 6 ($\chi = 4.3$) and 4 ($\chi = 3.1$). However, the scattering curves calculated from the monomeric structure (Fig. 3, gray solid lines) gives a worse fit to the scattering data at pH 6 ($\chi = 9.8$) and 4 ($\chi = 8.8$). Once again, it is clear that SAXS data for *Tp*BGL3 at pH 6 and 4 are consistent with homodimeric molecules in solution. The homodimeric high-resolution structure shows a particle with a D_{max} of 126.4 Å and $R_g = 37.68$ Å (Fig. 5b). These values are in a good agreement with results obtained by SAXS analysis (Table S2). The values calculated for the MM of *Tp*BGL3 at pH 6 and 4 using the SaxsmoW web tool (Fischer et al. 2010) were 148.40 and 158.10 kDa, respectively. In both cases, the results are consistent with a homodimeric molecule. In summary, our data using these methodologies indicate that both the enzymes were purified as homogeneous stable homodimers, and the oligomerization state of the *Tp*BGL1 and *Tp*BGL3 do not change in response to decreasing the pH from 6 to 4 at 20 °C.

The β-glucosidase structures remain well defined at acidic pH and below 80 °C

To correlate enzymatic activity with the structure of the enzymes, we conducted a series of detailed studies of the structural stability of the *Tp*BGL1 and *Tp*BGL3 at acidic pH, employing a series of biophysical techniques. CD spectroscopy was used to probe the secondary structure of the *Tp*BGL1 and *Tp*BGL3 at acidic pH. The CD spectra of *Tp*BGL1 measured at pH 6 and 4 are shown in Fig. 7a. The spectra are typical of proteins containing elements of α-helical secondary structure, as is expected based on the known structures of the GH1 β-glucosidases (Zechel et al. 2003; Cairns and Esen 2010). The results indicate that the secondary structure of the *Tp*BGL1 does not change significantly in response to decreasing the pH from 6 to 4 at 20 °C. Nevertheless, *Tp*BGL1 thermostability was found to be pH dependent. The thermostability of the *Tp*BGL1 was monitored following changes in the CD ellipticity at 222 nm. For *Tp*BGL1 at pH 6, the ellipticity at 222 nm remains relatively constant at temperatures lower than 90 °C, however, a small decrease was observed at temperatures higher than 90 °C (Fig. 7b). These small alterations observed at temperatures higher than 90 °C can be correlated with the loss of regular secondary structure. Furthermore, *Tp*BGL1 at pH 6 could not be completely unfolded at 100 °C. For *Tp*BGL1 at pH 4, the ellipticity at 222 nm remains relatively constant at temperatures lower than 80 °C, however, a progressive decrease was observed when the temperature was increased above 80 °C (Fig. 7b). These alterations observed at pH 4 indicated that *Tp*BGL1 drastically loses regular secondary structure at temperatures higher than 80 °C with a complete unfolding at 100 °C

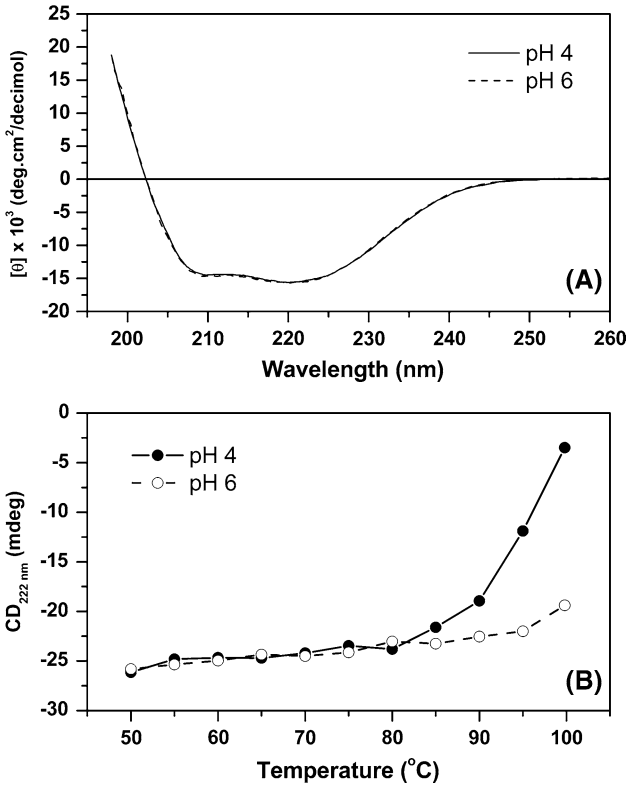

Fig. 7 Effect of pH on the secondary structure of *Tp*BGL1 monitored by far-UV CD spectroscopy. **a** Far-UV CD spectra as a function of pH. The pH values were 6 (*dash line*) and 4 (*solid line*). **b** Recombinant *Tp*BGL1 thermally unfolding monitored by far-UV CD at pH 6 (*open circle*) and 4 (*filled circle*). The experimental conditions are described in "Materials and methods"

(Fig. S4). At both pH values, the processes were essentially irreversible, in the conditions described here (data not shown).

The CD spectra of purified *Tp*BGL3 measured at pH 6 and 4 are shown in Fig. 8a. The spectra are typical of proteins with a mixed α/β structure as is expected based on the known structures of the GH3 β-glucosidases (Cairns and Esen 2010; Pozzo et al. 2010; McAndrew et al. 2013). These results exclude any effect on the regular secondary structure in response to increasing the pH from 4 to 6 at 20 °C. For *Tp*BGL3 at both pH 6 and 4, the ellipticities at 222 nm remain relatively constant at temperatures lower than 90 °C (Fig. 8b). However, a decrease in the ellipticities at 222 nm was observed at temperatures higher than 90 °C, suggesting a loss of regular secondary structure. At both pH values *Tp*BGL3 could be thermally denatured at 100 °C and the processes were essentially irreversible in the conditions described in this study (data not shown).

As a next step, the tertiary structure of *Tp*BGL1 and *Tp*BGL3 were investigated as a function of temperature by DLS. Figure 2 shows the variation of R_s as a function of temperature for *Tp*BGL1 and *Tp*BGL3 at two different pH

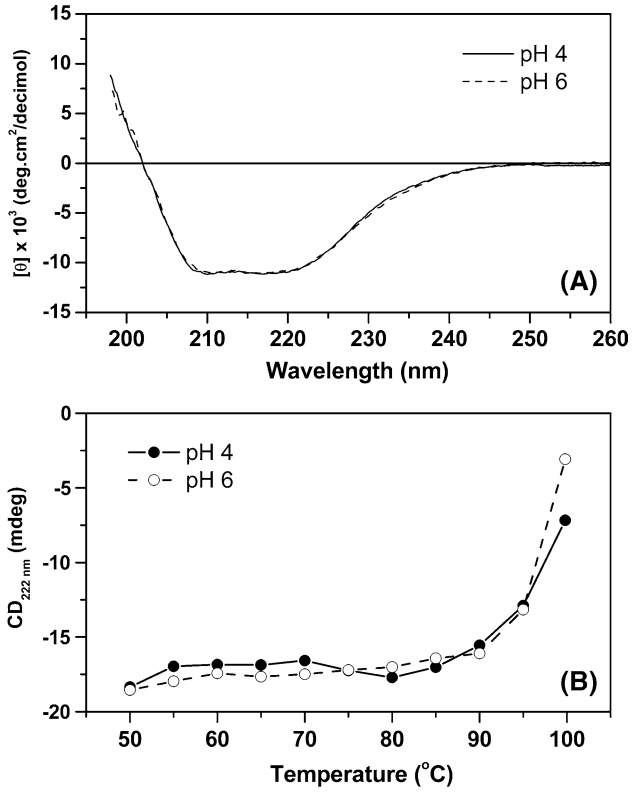

Fig. 8 Effect of pH on the secondary structure of *Tp*BGL3 monitored by far-UV CD spectroscopy. **a** Far-UV CD spectra as a function of pH. The pH values were 6 (*dash line*) and 4 (*solid line*). **b** Recombinant *Tp*BGL3 thermally unfolding monitored by far-UV CD at pH 6 (*open circle*) and 4 (*filled circle*). The experimental conditions are described in "Materials and methods"

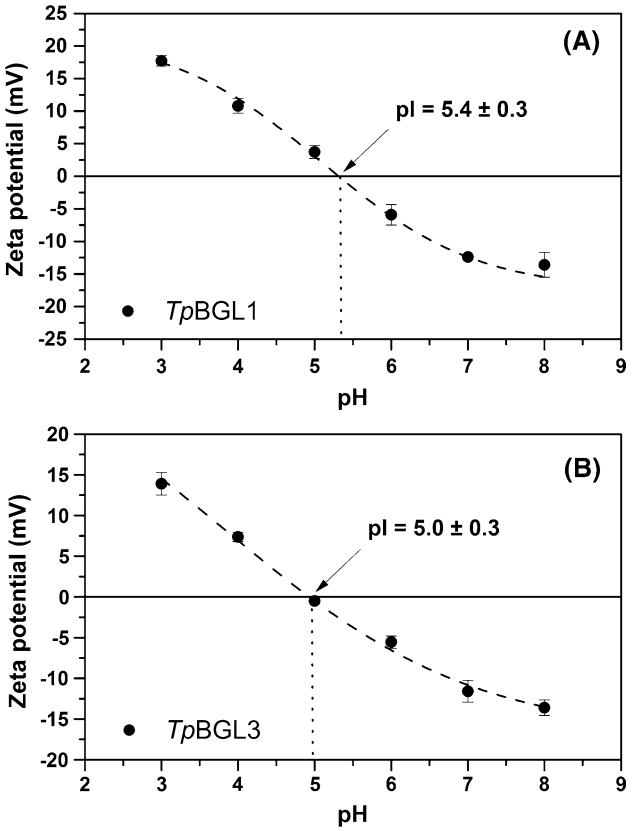

Fig. 9 Zeta potential. **a** Zeta potential of *Tp*BGL1 as a function of pH. **b** Zeta potential of *Tp*BGL3 as a function of pH. The symbols correspond to the experimental data, and the *dash lines* are just a guide for the eye

values. As can be seen, the R_s of *Tp*BGL1 exhibited minimal temperature dependence over the range 20–90 °C at pH 6 (Fig. 2a). However, when *Tp*BGL1 a pH 6 was incubated at 100 °C during 5 min and subsequently cooling back to 20 °C, the R_s obtained was approximately 20 nm, which corresponds to high molecular mass aggregates. At pH 4 the R_s also was practically independent on temperature over the range 20–75 °C. However, when *Tp*BGL1 at pH 4 was incubated at temperature values above 75 °C the R_s increased significantly, suggesting the appearance of amorphous aggregates as a result of the denaturation process (Fig. 2a). At both pH 6 and 4, the R_s of *Tp*BGL3 exhibited minimal temperature dependence over the range 20–90 °C (Fig. 2b). However, when *Tp*BGL3 was incubated in both pH values at 100 °C during 5 min and subsequently cooling back to 20 °C, the R_s values obtained increased significantly (approximately 25 nm), suggesting the appearance of aggregates. In all cases, the observed processes were essentially irreversible, in the conditions described here (data not shown). The DLS data are in agreement with circular dichroism results described above. Taken together, the results indicated that at acidic pH there were no significant changes in the secondary, tertiary and quaternary structures of the enzymes at temperatures below 80 °C, which could be detected by the biophysical techniques used in this study.

Influence of the net charge on the structural stability and enzymatic activity

Previous study indicates enzymes which activity is directly related by the balance between protonation and conformational changes (Bu et al. 2013). Interestingly, at acidic pH, our results indicated that there were no significant changes in the structures of the β-glucosidases at temperatures below 80 °C. Thus, the observed changes in the activity (Fig. 1) were due to variations in pH that modify protonation of the enzymes residues and the net charge, directly affecting the interactions with ligands. Ionic groups are involved in enzyme catalysis, such as the acid–base residue in the β-glucosidase active site. Thus, protonation state of the carboxylic acid residue and the carboxylate nucleophile is essential for enzymatic reaction, therefore, a pH variation

could impair the catalytic mechanism (Gitlin et al. 2006; Sørensen et al. 2013). To better understand the influence of pH on the number of uncompensated charges (N_c), the zeta potential of the β-glucosidases were determined as a function of pH (Figs. 9, S5). As can be seen in Fig. 9a, the zeta potential of *Tp*BGL1 decreased from 17.7 ± 0.8 mV at pH 3 to −13.6 ± 1.9 mV at pH 8. For *Tp*BGL3, the zeta potential was 13.9 ± 1.3 mV at pH 3 and −13.6 ± 0.9 mV at pH 8 (Fig. 9b). Zeta potential values were close to zero at pH 5.4 ± 0.3 for *Tp*BGL1 and pH 5.0 ± 0.3 for *Tp*BGL3. The results are in a good agreement with the theoretical isoelectric point values calculated from the amino acid sequences (5.6 and 5.3 for *Tp*BGL1 and *Tp*BGL3, respectively) (Gasteiger et al. 2003). The experimental values of the electrophoretic mobility and the net number of uncompensated charges per molecule are shown in Table 1.

In a previous study we have determined the optimal pH values for *Tp*BGL1 (pH 6, $K_m = 0.28 \pm 0.02$ mM, $k_{cat}/K_m = 999.28 \pm 166.59$ s^{-1} mM^{-1}) and *Tp*BGL3 (pH 4, $K_m = 0.38 \pm 0.03$ mM, $k_{cat}/K_m = 1490.43 \pm 348.53$ s^{-1} M^{-1}) at 70 °C (Cota et al. 2015). The net charge acquired at pH 6 ($N_C = -2.3$) is not sufficient to destabilize the secondary and tertiary structures of the *Tp*BGL1 even at temperatures between 80 and 90 °C (Figs. 7b, 2a). However, alterations at both secondary and tertiary structural levels were observed at pH 4 and temperatures above 80 °C (Figs. 7b, 2a). The net charge acquired at pH 4 ($N_C = 4.3$) by *Tp*BGL1 can influence their equilibrium properties such as the free energy of their interactions with ligands (Gitlin et al. 2006), while leading to structural destabilization only at temperatures higher than 80 °C. Also, it can be seen that at pH 4 the increase in temperature does not induce *Tp*BGL1 dissociation prior to denaturation (Fig. 2a). The increase in R_s indicates that aggregates are instantaneously formed upon denaturation, likely due to hydrophobic patches from different unfolded proteins associating with one another. Taken together, the results indicate that at temperatures between 80 and 90 °C, *Tp*BGL1 is more unstable at pH 4 than pH 6, probably due to the higher positive net charge acquired at pH 4 ($N_c = 4.3$) when compared with the same enzyme at pH 6 ($N_c = -2.3$). The larger positive net charge acquired at pH 4, which causes repulsion between charged groups, associated with temperatures above 80 °C destabilizes the enzyme. These two factors are likely to be responsible by the structural alterations observed that led to the formation of aggregates (Fig. 2a).

In contrast, the net charges acquired at pH 4 ($N_c = 3.3$) and 6 ($N_c = -2.3$) are not sufficient to destabilize the secondary and tertiary structures of the *Tp*BGL3 even at temperatures between 80 and 90 °C (Figs. 2b, 8b). The net charge acquired at both pH values by *Tp*BGL3 directly affects its enzymatic activity, however, causing structural destabilization only at temperatures higher 90 °C.

Table 1 Electrophoretic mobility (μ_c) and the number of uncompensated charges (N_c) for *Tp*BGL1 and *Tp*BGL3

pH	μ_c (μm cm Vs^{-1})	R_s (nm)	N_c
*Tp*BGL1			
3	1.4 ± 0.1	4.4 ± 0.1	6.5 ± 0.5
4	0.9 ± 0.1	4.5 ± 0.3	4.3 ± 0.5
5	0.3 ± 0.1	4.5 ± 0.1	1.4 ± 0.5
6	−0.5 ± 0.1	4.3 ± 0.3	−2.3 ± 0.5
7	−1.0 ± 0.1	4.6 ± 0.2	−4.8 ± 0.5
8	−1.1 ± 0.2	4.4 ± 0.2	−5.1 ± 0.9
*Tp*BGL3			
3	1.1 ± 0.1	5.7 ± 0.2	6.6 ± 0.6
4	0.6 ± 0.1	5.3 ± 0.2	3.3 ± 0.6
5	−0.1 ± 0.1	5.5 ± 0.2	−0.6 ± 0.6
6	−0.4 ± 0.1	5.5 ± 0.3	−2.3 ± 0.6
7	−0.9 ± 0.1	5.4 ± 0.2	−5.1 ± 0.6
8	−1.1 ± 0.1	5.6 ± 0.3	−6.5 ± 0.6

Conclusion

The present study provides new insight into the temperature and pH dependence of the structure of two different hyperthermostable β-glucosidases and how it correlates with the activity of the enzymes. Enzymatic activity is directly related to the balance between protonation and conformational changes. Interestingly, our results indicated that there were no significant changes in the secondary, tertiary and quaternary structures of the β-glucosidases at temperatures below 80 °C. Furthermore, the results indicated that both the enzymes are stable homodimers in solution. Therefore, the observed changes in the enzymatic activities are due to variations in pH that modify protonation of the enzyme residues and the net charge, directly affecting the interactions with ligands. Finally, the results showed that the two β-glucosidases displayed different pH dependence of thermostability at temperatures above 80 °C. *Tp*BGL1 showed higher stability at pH 6 than at pH 4, while *Tp*BGL3 showed similar stability at both pH values.

The biodegradation of lignocellulosic biomass involves a concerted attack by several enzymes, including β-glucosidases as key component. Current methodologies for biomass conversion to biofuels employ physical and/or chemical pretreatments that disrupt the lignocellulosic biomass in plant cell walls in combination with enzymatic hydrolysis of the cellulose to produce free sugars (Rezende et al. 2011; Jiang et al. 2013). Thus, stable cellulolytic enzymes with high enzymatic activity in pretreatment biomass conditions, including high temperatures and acidic conditions, are likely to be essential at an industrial scale production. These two features make *Tp*BGL1 and *Tp*BGL3 enzymes to be of significant biotechnological interest.

Acknowledgments We would like to thank the National Synchrotron Light Laboratory (LNLS, Brazil) and CENAPAD-SP (Centro Nacional de Processamento de Alto Desempenho em São Paulo). The authors would like to thank FAPESP and CNPq for the financial support for this work via grants # 2012/21054-9, # 478900/2012-0, # 2008/58037-9 and # 2011/13242-7; and fellowships # 2012/03503-0 (VMS) and # 501037/2012-8 (FC).

Conflict of interest The authors declare that they do not have competing interests.

References

Aguilar CF, Sanderson I, Moracci M, Ciaramella M, Nucci R, Rossi M, Pearl LH (1997) Crystal structure of the β-glycosidase from the hyperthermophilic archeon *Sulfolobus solfataricus*: resilience as a key factor in thermostability. J Mol Biol 271:789–802

Arnold K, Bordoli L, Kopp J, Schwede T (2006) The Swiss-model workspace: a web-based environment for protein structure homology modelling. Bioinformatics 22:195–201

Bu L, Crowley MF, Himmel ME, Beckham GT (2013) Computational investigation of the pH dependence of loop flexibility and catalytic function in glycoside hydrolases. J Biol Chem 288:12175–12186

Cairns JRK, Esen A (2010) β-Glucosidases. Cell Mol Life Sci 67:3389–3405

Chi YI, Martinez-Cruz LA, Jancarik J, Swanson RV, Robertson DE, Kim SH (1999) Crystal structure of the beta-glycosidase from the hyperthermophile *Thermosphaera aggregans*: insights into its activity and thermostability. FEBS Lett 445:375–383

Colussi F, Garcia W, Rosseto FR, Mello BLS, Oliveira Neto M, Polikarpov I (2012) Effect of pH and temperature on the global compactness, structure, and activity of cellobiohydrolase Cel7A from *Trichoderma harzianum*. Eur Biophys J 41:89–98

Cota J, Alvarez TM, Citadini AP, Santos CR, Oliveira Neto M, Oliveira RR, Pastore GM, Ruller R, Prade RA, Murakami MT, Squina FM (2011) Mode of operation and low resolution structure of a multi-domain and hyperthermophilic endo-β-1,3-glucanase from Thermotoga petrophila. Biochem Biophys Res Commun 406:590–594

Cota J, Corrêa TLR, Damásio ARL, Diogo JA, Hoffmam ZB, Garcia W, Oliveira LC, Prade RA, Squina FM (2015) Comparative analysis of three hyperthermophilic GH1 and GH3 family members with industrial. New Biotechnol 32(1):13–20

Dias CA, Garcia W, Zanelli CF, Valentini SR (2013) eIF5A dimerizes not only in vitro but also in vivo and its molecular envelope is similar to the EF-P monomer. Amino Acids 44(2):631–644

Fischer H, de Oliveira Neto M, Napolitano HB, Polikarpov I, Craievich AF (2010) Determination of the molecular weight of proteins in solution from single small-angle X-ray scattering measurement on a relative scale. J Appl Cryst 43:101–109

Gasteiger E, Gattiker A, Hoogland C, Ivanyi I, Appel RD, Bairoch A (2003) ExPASy: the proteomics server for in-depth protein knowledge and analysis. Nucleic Acids Res 31:3784–3788

Gitlin I, Carbeck JD, Whitesides GM (2006) Why are proteins charged? Networks of charge-charge interactions in proteins measured by charge ladders and capillary electrophoresis. Angew Chem Int Ed Engl 45:3022–3060

Hall M, Rubin J, Behrens SH, Bommarius AS (2011) The cellulose-binding domain of cellobiohydrolase Cel7A from *Trichoderma reesei* is also a thermostabilizing domain. J Biotechnol 155:370–376

Jachimska B, Wasilewska M, Adamczyk Z (2008) Characterization of globular protein solutions by dynamic light scattering, electrophoretic mobility, and viscosity measurements. Langmuir 24:6866–6872

Jiang F, Kittle JD, Tan X, Esker AR, Roman M (2013) Effects of sulfate groups on the adsorption and activity of cellulases on cellulose substrates. Langmuir 29:3280–3291

Kado Y, Inoue T, Ishikawa K (2011) Structure of hyperthermophilic β-glucosidase from *Pyrococcus furiosus*. Acta Cryst F 67:1473–1479

Krissinel E, Henrick K (2007) Inference of macromolecular assemblies from crystalline state. J Mol Biol 372:774–797

Kumar R, Singh S, Singh OV (2008) Bioconversion of lignocellulosic biomass: biochemical and molecular perspectives. J Ind Microbiol Biotechnol 35:377–391

Lombard V, Golaconda RH, Drula E, Coutinho PM, Henrissat B (2013) The carbohydrate-active enzymes database (CAZy) in 2013. Nucleic Acids Res 42:D490–D495

Lundemo P, Adlercreutz P, Karlsson EN (2013) Improved transferase/hydrolase ratio through rational design of a family 1 β-Glucosidase from *Thermotoga neapolitana*. Appl Environ Microbiol 79:3400–3405

Lynd LR, Weimer PJ, van Zyl WH, Pretorius IS (2002) Microbial cellulose utilization: fundamentals and biotechnology. Microbiol Mol Biol Rev 66:506–577

Lynd LR, Laser MS, Bransby D, Dale BE, Davison B, Hamilton R, Himmel M, Keller M, McMillan JD, Sheehan J, Wyman CE (2008) How biotech can transform biofuels. Nat Biotechnol 26:169–172

McAndrew RP, Park JI, Heins RA, Reindl W, Friedland GD, D'haeseleer P, Northen T, Sale KL, Simmons BA, Adams PD (2013) From soil to structure, a novel dimeric β-glucosidase belonging to glycoside hydrolase family 3 isolated from compost using metagenomic analysis. J Biol Chem 288:14985–14992

Nakatani Y, Cutfield SM, Cowieson NP, Cutfield JF (2012) Structure and activity of exo-1,3/1,4-β-glucanase from marine bacterium *Pseudoalteromonas* sp. BB1 showing a novel C-terminal domain. FEBS J 279:464–478

Pozzo T, Pasten JL, Karlsson EN, Logan DT (2010) Structural and functional analyses of β-glucosidase 3B from *Thermotoga neapolitana*: a thermostable three-domain representative of glycoside hydrolase 3. J Mol Biol 397:724–739

Rezende CA, de Lima MA, Maziero P, Deazevedo ER, Garcia W, Polikarpov I (2011) Chemical and morphological characterization of sugarcane bagasse submitted to a delignification process for enhanced enzymatic digestibility. Biotechnol Biofuels 4:54

Santiago PS, Carvalho FAO, Domingues MM, Carvalho JW, Santos NC, Tabak M (2010) Isoelectric point determination for *Glossoscolex paulistus* extracellular hemoglobin: oligomeric stability in acidic pH and relevance to protein-surfactant interactions. Langmuir 26:9794–9801

Santos CR, Squina FM, Navarro AM, Oldiges DP, Leme AF, Ruller R, Mort AJ, Prade R, Murakami MT (2011) Functional and biophysical characterization of hyperthermostable GH5 a-L-arabinofuranosidase from *Thermotoga petrophila*. Biotechnol Lett 33:131–137

Santos CR, Paiva JH, Meza AN, Cota J, Alvarez TM, Ruller R, Prade RA, Squina FM, Murakami MT (2012) Molecular insights into substrate specificity and thermal stability of a bacterial GH5-CBM27 endo-1,4-β-D-mannanase. J Struct Biol 177:469–476

Shewale JG (1982) β-Glucosidase: its role in cellulase synthesis and hydrolysis of cellulose. Int J Biochem 14:435–443

Silva VM, Colussi F, Oliveira Neto M, Braz A, Squina MF, Oliveira CL, Garcia W (2014) Modular hyperthermostable bacterial endo-β-1,4-Mannanase: molecular shape, flexibility and temperature-dependent conformational changes. Plos One 9(3):e92996

Sørensen A, Lübeck M, Lübeck PS, Ahring BK (2013) Fungal β-glucosidases: a bottleneck in industrial use of lignocellulosic materials. Biomolecules 3:612–631

Squina FM, Prade RA, Wang H, Murakami MT (2009) Expression, purification, crystallization and preliminary crystallographic analysis of an endo-1,5-α-L-arabinanase from hyperthermophilic *Thermotoga petrophila*. Acta Crystallogr Sect F 65:902–905

Suzuki K, Sumitani J, Nam Y, Nishimaki T, Tani S, Wakagi T, Kawaguchi T, Fushinobu S (2013) Crystal structures of glycoside hydrolase family 3 β-glucosidase 1 from *Aspergillus aculeatus*. Biochem J 452:211–221

Svergun DI (1992) Determination of the regularization parameter in indirect-transform methods using perceptual criteria. J Appl Cryst 25:495–503

Svergun DI, Barberato C, Koch MHJ (1995) CRYSOL—a program to evaluate X-ray solution scattering of biological macromolecules from atomic coordinates. J Appl Cryst 28:768–773

Takahata Y, Nishijima M, Hoaki T, Maruyama T (2001) *Thermotoga petrophila* sp. nov. and *Thermotoga naphthophila* sp. nov., Two hyperthermophilic bacteria from the Kubiki oil reservoir in Niigata Japan. Int J Syst Evol Microbiol 51:1901–1909

Tomovic A, Oakeley EJ (2008) Computational structural analysis: multiple proteins bound to DNA. PLoS One 3(9):e3243

Varghese JN, Hrmova M, Fincher GB (1999) Three-dimensional structure of a barley β-D-glucan exohydrolase, a family 3 glycosyl hydrolase. Structure 7:179–190

Xiao ZZ, Zhang X, Gregg DJ, Saddler JN (2004) Effects of sugar inhibition on cellulases and β-glucosidase during enzymatic hydrolysis of softwood substrates. Appl Biochem Biotechnol 113:1115–1126

Yoshida E, Hidaka M, Fushinobu S, Koyanagi T, Minami H, Tamaki H, Kitaoka M, Katayama T, Kumagai H (2010) Role of a PA14 domain in determining substrate specificity of a glycoside hydrolase family 3 β-glucosidase from *Kluyveromyces marxianus*. Biochem J 431:39–49

Zechel DL, Boraston AB, Gloster TM, Boraston CM, Macdonald JM, Tibrook DM, Stick RV, Davies GJ (2003) Iminosugar glycosidase inhibitors: structural and thermodynamic dissection of the binding of isofagomine and 1-deoxynojirimycin to β-glucosidases. J Am Chem Soc 125:14313–14323